Available online at http://scik.org
Eng. Math. Lett. 2025, 2025:1
https://doi.org/10.28919/eml/8936
ISSN: 2049-9337

DEVELOPMENT AND ANALYSIS OF A NUMERICAL MODEL FOR INCOMPRESSIBLE FLOW IN OPEN CIRCULAR CHANNELS AND ITS APPLICATION

EMMANUEL AKALIGWO[1,*], BONIFACE AHARANWA[2], EKENE AZUBUKO[1], JOSEPH NWOKE[1], TONY OGALA[1], MUSTAPHA MICHAEL[1]

[1]Department of Mathematics, Federal University Lokoja, Kogi State, Nigeria

[2]Department of Mathematics/Statistics, Imo State Polytechnic, Omuma, Imo State, Nigeria

Copyright © 2025 the author(s). This is an open access article distributed under the Creative Commons Attribution License, which permits unrestricted use, distribution, and reproduction in any medium, provided the original work is properly cited.

Abstract. Amidst the escalating challenges posed by nationwide flooding during the rainy season, exacerbated by the El Niño phenomenon, there is an urgent need for improved water management systems. Open circular channels play a crucial role in flood control, irrigation, and water supply networks. However, optimizing the flow efficiency in these channels remains a significant challenge, especially when considering the complex interplay between key parameters like depth, velocity, and pressure. This study aims to develop a sophisticated mathematical model that addresses these challenges, offering a tool for enhancing the operational efficiency of open circular channels. The proposed model based on the RANS equations for incompressible flow, integrated with the EARSM turbulence model and solved using the artificial compressibility method, offers a robust framework for simulating complex turbulent flows. The application of implicit finite volume discretization ensures that the model is stable and accurate, while the boundary conditions allow for realistic and detailed simulations of practical fluid flow scenarios.

Keywords: incompressible flow; open circular channels; finite difference method; flow dynamics; flood mitigation.

2020 AMS Subject Classification: 76M30,76D05, 76M20, 76D07.

*Corresponding author

E-mail address: emmanuel.akaligwo@fulokoja.edu.ng

Received October 01, 2024

1. INTRODUCTION

Recent extreme weather events, including prolonged rains and the ongoing El Niño phenomenon, have led to severe flooding across northern and southern regions of the country. This crisis follows a recent recovery from severe drought, highlighting a vulnerability in water management systems. In Lagos State, for example water flowing from highlands to lowlands causes existing channels to overflow, leading to extensive urban flooding and stagnant water. Informal settlements, already prone to flooding even during average rainfall, are particularly affected [16, 15, 18]. This situation underscores the urgent need for well-designed channels that can handle stormwater efficiently, prevent urban flooding, and redirect excess water to agricultural lands [8, 13, 16, 19]. Channels are classified as open or closed based on their top structure. Open channels, such as rivers and streams, have uncovered tops and can be designed with various cross-sections, including trapezoidal, rectangular, and circular. Closed channels, or conduits, are covered and include pipes and tunnels [2, 6, 9, 10]. Effective stormwater management relies heavily on understanding and designing open channels, which involves studying the forces of gravity, viscosity, and inertia that govern flow dynamics. A number of studies have explored various aspects of open channel flow, particularly in channels with circular cross-sections (see [14, 9, 8, 4, 11]). The study of incompressible flow in open water channels is crucial for various engineering applications, including irrigation, drainage systems, flood control, and hydraulic engineering. Understanding the behavior of fluid flow in open channels under incompressible conditions provides insights into optimizing these systems for efficiency and stability. This review summarizes recent advancements and methodologies in modeling incompressible flow in open channels, focusing on turbulence mitigation, mathematical modeling, and computational fluid dynamics (CFD). Turbulence plays a significant role in the dynamics of incompressible flow within open channels. [5] explored the mitigation of flow turbulence using $X-$shaped vanes in an open channel. Their study focused on simulating and analyzing water flow in two dimensions (2D), considering the flow as incompressible. The introduction of vanes effectively reduced turbulence intensity, which is critical in maintaining stable flow conditions in engineering applications. [15] conducted a study on the mathematical modeling of fluid flow in open circular channels within sewerage systems. Their research focused on the flow dynamics of an

incompressible Newtonian fluid in artificial rectangular channels, incorporating lateral inflows. The mathematical approach adopted in this study allowed for the prediction of flow patterns and the identification of potential issues, such as backwater effects and flow separations, which are critical in the design and management of open channel systems. CFD simulations have become a powerful tool in studying incompressible flow in open channels, allowing for detailed analysis of complex flow patterns and interactions. [11] investigated turbulent heat transfer structures in open channels using large eddy simulation (LES) techniques. Their research demonstrated the applicability of open-source CFD codes in modeling incompressible flow, with a focus on optimizing heat transfer efficiency. The study highlighted the importance of selecting appropriate modeling options for accurately capturing the nuances of turbulent flow in open channels. Similarly, [7] explored the behavior of shallow water flows with discontinuous topography using incompressible fluid models. Their work emphasized the challenges posed by topographical variations in open channel flow and the necessity of incorporating these factors into CFD models for accurate predictions. The use of incompressible flow assumptions in their study allowed for a more straightforward analysis of the fluid dynamics involved, making it easier to apply the findings to practical engineering problems. The study of incompressible flow in open channels has significant implications for hydraulic engineering. [17] conducted a numerical investigation of turbulence models for vegetated channel flows, using CFD simulations to calculate velocity fields. This research provides a foundation for incorporating turbulence-mitigation strategies in the design of open water channels, emphasizing the importance of controlling flow behavior to enhance channel performance. Mathematical models are essential for predicting the behavior of incompressible flows in open channels. The findings of this study contribute to the development of more accurate models for predicting flow behavior, which is essential for effective water resource management.

1.1. Governing Equations. The governing equations for incompressible flow in an open water channel are typically derived from the Navier-Stokes equations under the assumption of incompressibility. The key equations include the continuity equation and the momentum equation. For an incompressible fluid, the modified continuity equation becomes:

$$\beta^2 \frac{\partial p}{\partial t} + \nabla \cdot \mathbf{u} = 0 \tag{1}$$

Where β is the artificial compressibility parameter. This term allows for the pressure to propagate through the domain while solving for incompressible flow. For an incompressible Newtonian fluid, the Navier-Stokes equation in three dimensions is

$$\rho \left(\frac{\partial \mathbf{u}}{\partial t} + \mathbf{u} \cdot \nabla \mathbf{u} \right) = -\nabla p + \mu \nabla^2 \mathbf{u} + \mathbf{f} \tag{2}$$

where $\mathbf{u} = (u, v, w)$ is the velocity vector, ρ is the fluid density, p is the pressure, μ is the dynamic viscosity, $\mathbf{f}$ represents body forces (e.g., gravity). This equation (1) ensures the incompressibility condition, implying that the fluid density is constant and the flow is divergence-free. Given that real-world flows often exhibit turbulence, the Navier-Stokes equations need to be modified or supplemented by a turbulence model. Common approach includes Reynolds-Averaged Navier-Stokes (RANS) Equations

$$\rho \left(\frac{\partial \overline{\mathbf{u}}}{\partial t} + \overline{\mathbf{u}} \cdot \nabla \overline{\mathbf{u}} \right) = -\nabla \overline{p} + \mu \nabla^2 \overline{\mathbf{u}} + \nabla \cdot \left(\rho \overline{\mathbf{u}' \mathbf{u}'} \right) + \mathbf{f} \tag{3}$$

Here, the velocity $\mathbf{u}$ and pressure p are decomposed into mean ($\overline{\mathbf{u}}$, $\overline{p}$) and fluctuating components ($\mathbf{u}'$, p'). The term $\rho \overline{\mathbf{u}' \mathbf{u}'}$ represents the Reynolds stress, which is modeled using turbulence models like k-ε or k-ω. The effect of non-uniform bed roughness can be incorporated by modifying the boundary conditions and introducing a roughness parameter, often represented by the Nikuradse equivalent sand roughness k_s. Momentum Equation (RANS)

$$\rho \left(\frac{\partial \mathbf{u}}{\partial t} + \mathbf{u} \cdot \nabla \mathbf{u} \right) = -\nabla p + \mu \nabla^2 \mathbf{u} - \nabla \cdot \tau_{\text{turbulent}}$$

Where: ρ is the fluid density, p is the pressure, μ is the dynamic viscosity, $\tau_{\text{turbulent}}$ is the Reynolds stress tensor, accounting for the effects of turbulence. The Wall Shear Stress is

$$\tau_w = \rho \left(C_f \frac{|\overline{\mathbf{u}}| \overline{\mathbf{u}}}{2} \right) \tag{4}$$

where C_f is a friction coefficient that accounts for roughness and is a function of k_s. For open channel flows, the free surface is an important boundary condition, governed by

$$\frac{\partial \eta}{\partial t} + \overline{\mathbf{u}} \cdot \nabla \eta = w \tag{5}$$

where η is the surface elevation and w is the vertical velocity component at the free surface. Dynamic Boundary Condition

$$p = p_{\text{atm}} \quad \text{at } y = \eta \tag{6}$$

where p_{atm} is the atmospheric pressure at the free surface. If heat transfer or thermal effects are considered:

$$\rho c_p \left(\frac{\partial T}{\partial t} + \mathbf{u} \cdot \nabla T \right) = k \nabla^2 T + \Phi \tag{7}$$

where T is the temperature, c_p is the specific heat at constant pressure, k is the thermal conductivity, Φ is the viscous dissipation function. The general form of the Reynolds stress tensor $\tau_{\text{turbulent}}$ in the Explicit Algebraic Reynolds Stress Model (EARSM) model is:

$$\tau_{\text{turbulent}} = \rho \overline{u_i' u_j'} = 2 \nu_t S_{ij} - \frac{2}{3} \rho k \delta_{ij} \tag{8}$$

where S_{ij} is the mean strain rate tensor, ν_t is the eddy viscosity, k is the turbulent kinetic energy and δ_{ij} is the Kronecker delta. These equations (1) - (8) collectively describe the behavior of incompressible flow in open circular channels, capturing the effects of turbulence, bed roughness, and non-linearities inherent in real-world flows.

1.2. Non-dimensionalization of the governing equations. To non-dimensionalize the governing equations, we first choose characteristic scales for the variables involved,Length scale L (e.g., channel width or depth), Velocity scale U (e.g., typical flow speed),Time scale $T = \frac{L}{U}$, Pressure scale $P = \rho U^2$, Height scale H (e.g., characteristic water depth). Using the characteristic scales, we define the non-dimensional variables Starting from the incompressible Navier-Stokes equation

$$\rho \left(\frac{\partial \mathbf{u}}{\partial t} + \mathbf{u} \cdot \nabla \mathbf{u} \right) = -\nabla p + \mu \nabla^2 \mathbf{u} + \mathbf{f}$$

Substitute the non-dimensional variables

$$\rho \left(\frac{U}{L} \frac{\partial \mathbf{u}^*}{\partial t^*} + \frac{U^2}{L} \mathbf{u}^* \cdot \nabla^* \mathbf{u}^* \right) = -\frac{P}{L} \nabla^* p^* + \mu \frac{U}{L^2} \nabla^{*2} \mathbf{u}^* + \mathbf{f}^*$$

Now, divide through by the dynamic pressure scale $\rho U^2 / L$

$$\frac{\partial \mathbf{u}^*}{\partial t^*} + \mathbf{u}^* \cdot \nabla^* \mathbf{u}^* = -\nabla^* p^* + \frac{\mu}{\rho U L} \nabla^{*2} \mathbf{u}^* + \frac{\mathbf{f}^*}{\rho U^2}$$

Here, the dimensionless group $\frac{\mu}{\rho UL}$ is the inverse Reynolds number $\frac{1}{Re}$, where $Re = \frac{\rho UL}{\mu}$. The body force term is usually represented as a gravitational force, which is $\mathbf{f} = \rho\mathbf{g}$. Non-dimensionalizing $\mathbf{g}$ gives a Froude number $Fr = \frac{U}{\sqrt{gL}}$. The non-dimensional momentum equation becomes

$$\frac{\partial \mathbf{u}^*}{\partial t^*} + \mathbf{u}^* \cdot \nabla^* \mathbf{u}^* = -\nabla^* p^* + \frac{1}{Re}\nabla^{*2}\mathbf{u}^* + \frac{1}{Fr^2}\mathbf{g}^*$$

The incompressible continuity equation is

$$\nabla \cdot \mathbf{u} = 0$$

Substituting the non-dimensional variables

$$\nabla^* \cdot \mathbf{u}^* = 0$$

This remains unchanged since the continuity equation is already non-dimensional. For the kinematic boundary condition at the free surface $y = \eta$

$$\frac{\partial \eta}{\partial t} + \mathbf{u} \cdot \nabla \eta = w$$

Non-dimensionalize this using

$$\frac{L}{U}\frac{\partial \eta^*}{\partial t^*} + U\mathbf{u}^* \cdot \frac{1}{L}\nabla^* \eta^* = U\frac{w^*}{L}$$

Simplifying

$$\frac{\partial \eta^*}{\partial t^*} + \mathbf{u}^* \cdot \nabla^* \eta^* = w^*$$

For non-uniform bed roughness

$$\tau_w = \rho C_f \frac{|\mathbf{u}|\mathbf{u}}{2}$$

where C_f can be non-dimensionalized based on k_s^*. These non-dimensional equations form the basis of the numerical model and can be used to analyze the effects of Reynolds number, Froude number, and wall roughness on the flow behavior in open circular channels.

1.3. Boundary Conditions. The model requires appropriate boundary conditions to simulate real-world scenarios. At the channel walls, the velocity of the fluid is zero relative to the wall. At the free surface of the flow, the pressure is atmospheric, and the velocity normal to the surface is zero. Boundary conditions should be applied as follows: At the boundaries (e.g., $r = 0$, $r = R$, $z = 0$, $z = L$). Apply Dirichlet (prescribed velocity or pressure) or Neumann (prescribed gradient) conditions based on the physical problem. Symmetry or axis boundary (e.g., at $r = 0$): $\frac{\partial u_z}{\partial r} = 0$ and $u_r = 0$.

1.4. Numerical Methods. Finite Difference Method (FDM) is employed to solve the governing equations. This method is chosen for its conservation properties and suitability for complex geometries. The discretized equations are solved using iterative solvers such as the SIMPLE (Semi-Implicit Method for Pressure-Linked Equations) algorithm. To find the Finite Difference Method (FDM) representation of the momentum equations in cylindrical coordinates, specifically in the r and z directions, we'll start by writing the momentum equations in their differential form and then discretize them using finite differences. The Navier-Stokes equations in cylindrical coordinates (r, θ, z) for incompressible flow are, r-direction (Radial):

$$\rho\left(\frac{\partial u_r}{\partial t} + u_r\frac{\partial u_r}{\partial r} + \frac{u_\theta}{r}\frac{\partial u_r}{\partial \theta} + u_z\frac{\partial u_r}{\partial z} - \frac{u_\theta^2}{r}\right) = -\frac{\partial p}{\partial r} + \mu\left(\nabla^2 u_r - \frac{u_r}{r^2} - \frac{2}{r^2}\frac{\partial u_\theta}{\partial \theta}\right)$$

z-direction (Axial)

$$\rho\left(\frac{\partial u_z}{\partial t} + u_r\frac{\partial u_z}{\partial r} + \frac{u_\theta}{r}\frac{\partial u_z}{\partial \theta} + u_z\frac{\partial u_z}{\partial z}\right) = -\frac{\partial p}{\partial z} + \mu\nabla^2 u_z$$

Here, u_r, u_θ, u_z are the velocity components in the r, θ, and z directions, respectively, ρ is the fluid density, μ is the dynamic viscosity, p is the pressure. We will discretize the equations using central differences for spatial derivatives and forward differences for time derivatives. Discretization in the r-direction: Radial velocity u_r,

$$\frac{\partial u_r}{\partial r} \approx \frac{u_r^{i+1,j,k} - u_r^{i-1,j,k}}{2\Delta r} \tag{9}$$

$$\frac{\partial^2 u_r}{\partial r^2} \approx \frac{u_r^{i+1,j,k} - 2u_r^{i,j,k} + u_r^{i-1,j,k}}{\Delta r^2} \tag{10}$$

Azimuthal velocity u_θ,

$$\frac{\partial u_\theta}{\partial \theta} \approx \frac{u_\theta^{i,j+1,k} - u_\theta^{i,j-1,k}}{2\Delta\theta} \tag{11}$$

$$\frac{\partial^2 u_\theta}{\partial \theta^2} \approx \frac{u_\theta^{i,j+1,k} - 2u_\theta^{i,j,k} + u_\theta^{i,j-1,k}}{\Delta\theta^2} \tag{12}$$

Axial velocity u_z,

$$\frac{\partial u_r}{\partial z} \approx \frac{u_r^{i,j,k+1} - u_r^{i,j,k-1}}{2\Delta z} \tag{13}$$

$$\frac{\partial^2 u_r}{\partial z^2} \approx \frac{u_r^{i,j,k+1} - 2u_r^{i,j,k} + u_r^{i,j,k-1}}{\Delta z^2} \tag{14}$$

Discretization in the z-direction, Axial velocity u_z,

$$\frac{\partial u_z}{\partial z} \approx \frac{u_z^{i,j,k+1} - u_z^{i,j,k-1}}{2\Delta z} \tag{15}$$

$$\frac{\partial^2 u_z}{\partial z^2} \approx \frac{u_z^{i,j,k+1} - 2u_z^{i,j,k} + u_z^{i,j,k-1}}{\Delta z^2} \tag{16}$$

Discretizing the radial momentum equation,

$$\begin{aligned}
\frac{\rho}{\Delta t}\left(u_r^{i,j,k} - u_r^{i,j,k-1}\right) &+ \rho\left(\frac{u_r^{i,j,k}\left(u_r^{i+1,j,k} - u_r^{i-1,j,k}\right)}{2\Delta r} + \frac{u_\theta^{i,j,k}\left(u_r^{i,j+1,k} - u_r^{i,j-1,k}\right)}{2r\Delta\theta}\right. \\
&\left. + \frac{u_z^{i,j,k}\left(u_r^{i,j,k+1} - u_r^{i,j,k-1}\right)}{2\Delta z} - \frac{u_\theta^{2,i,j,k}}{r}\right) \\
&= -\frac{p^{i+1,j,k} - p^{i-1,j,k}}{2\Delta r} + \mu\left(\frac{u_r^{i+1,j,k} - 2u_r^{i,j,k} + u_r^{i-1,j,k}}{\Delta r^2} + \frac{u_r^{i,j+1,k} - 2u_r^{i,j,k} + u_r^{i,j-1,k}}{r^2\Delta\theta^2}\right. \\
&\left. + \frac{u_r^{i,j,k+1} - 2u_r^{i,j,k} + u_r^{i,j,k-1}}{\Delta z^2} - \frac{u_r^{i,j,k}}{r^2} - \frac{2\left(u_\theta^{i,j+1,k} - u_\theta^{i,j-1,k}\right)}{r^2\Delta\theta}\right)
\end{aligned}$$

Discretizing the axial momentum equation:

$$\begin{aligned}
\frac{\rho}{\Delta t}\left(u_z^{i,j,k} - u_z^{i,j,k-1}\right) &+ \rho\left(\frac{u_r^{i,j,k}\left(u_z^{i+1,j,k} - u_z^{i-1,j,k}\right)}{2\Delta r} + \frac{u_\theta^{i,j,k}\left(u_z^{i,j+1,k} - u_z^{i,j-1,k}\right)}{2r\Delta\theta}\right. \\
&\left. + \frac{u_z^{i,j,k}\left(u_z^{i,j,k+1} - u_z^{i,j,k-1}\right)}{2\Delta z}\right) \\
&= -\frac{p^{i,j,k+1} - p^{i,j,k-1}}{2\Delta z} + \mu\left(\frac{u_z^{i+1,j,k} - 2u_z^{i,j,k} - u_z^{i-1,j,k}}{\Delta r^2}\right. \\
&\left. + \frac{u_z^{i,j+1,k} - 2u_z^{i,j,k} - u_z^{i,j-1,k}}{r^2\Delta\theta^2} + \frac{u_z^{i,j,k+1} - 2u_z^{i,j,k} - u_z^{i,j,k-1}}{\Delta z^2}\right)
\end{aligned}$$

These FDM approximations form the basis for solving the momentum equations in cylindrical coordinates, which is applicable to problems like pipe flow, flow in cylindrical containers, or axisymmetric flows.

2. Model Validation and Verification

The flow parameters of Reynold's and Froude's numbers were investigated to determine how they affect the velocity. The figure 1 illustrate the effects of Reynolds number on the velocity

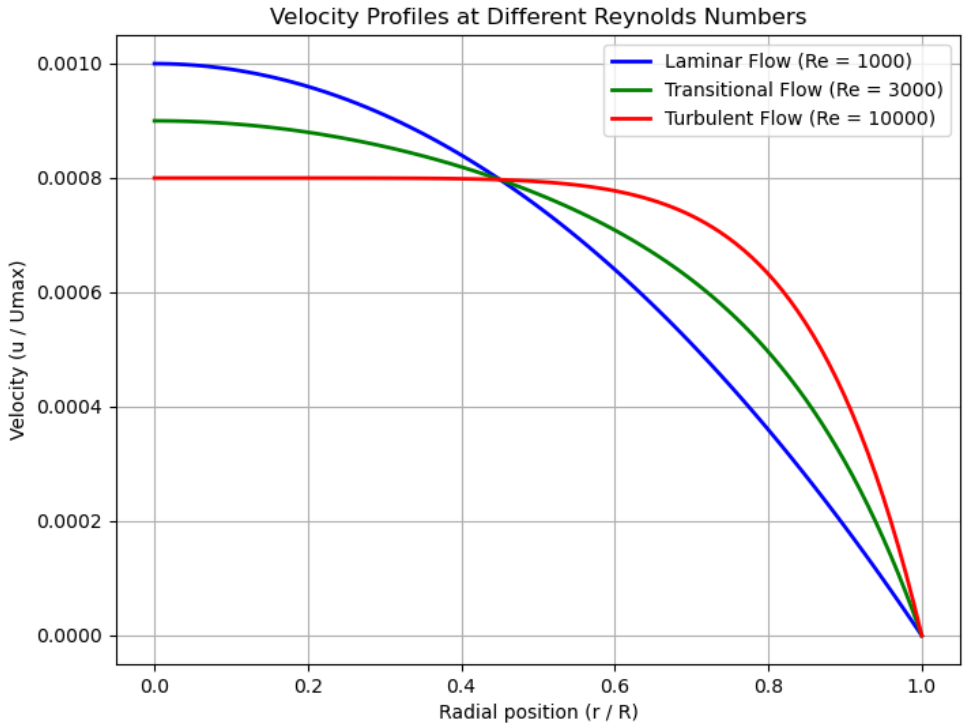

FIGURE 1. Effects of Reynolds number on the velocity Profiles

profiles for laminar and turbulent flows. The velocity profile is parabolic. The flow velocity is maximum at the center of the pipe and decreases smoothly to zero at the pipe walls. This is typical for low Reynolds numbers ($Re < 2000$), where viscous forces dominate, leading to smooth and orderly flow. The velocity profile in turbulent flow is flatter in the core region with a sharp gradient near the walls, typical of high Reynolds numbers ($Re > 4000$). The right graph uses a logarithmic scale to represent the velocity profile, showing how the velocity

changes rapidly near the wall (in the boundary layer) and remains relatively uniform in the central region. These visualizations clearly demonstrate how the Reynolds number affects the shape of velocity profiles, transitioning from a smooth parabolic profile in laminar flow to a flatter, more complex profile in turbulent flow. The figure 2 shows that the velocity profile in an

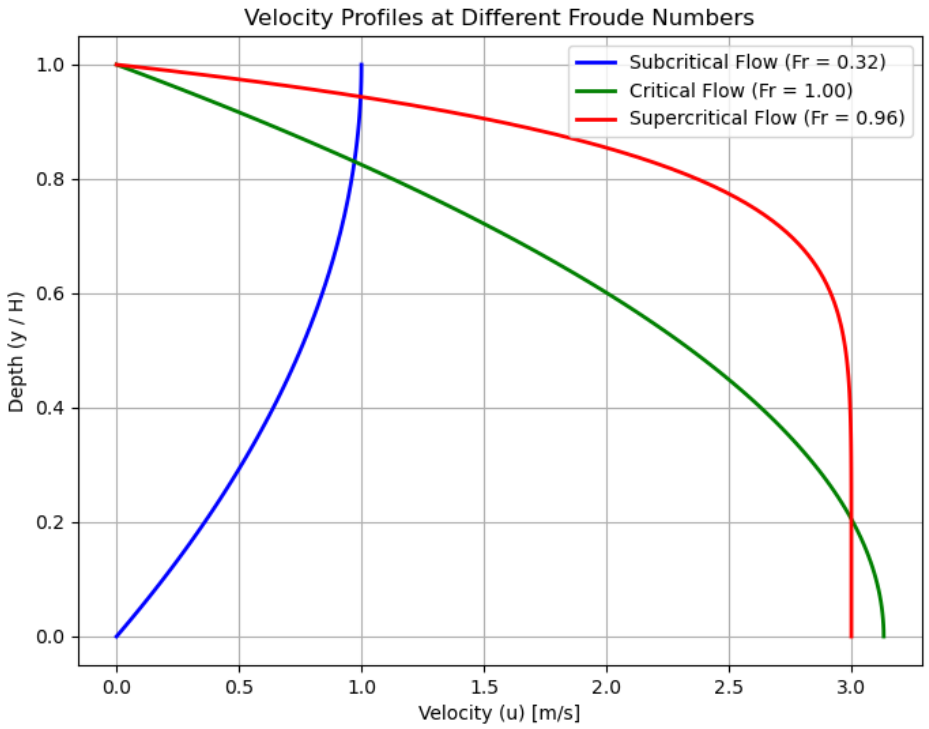

FIGURE 2. Effects of Froude's number on the velocity Profiles

open circular channel is strongly influenced by the Froude's number. As the Froude's number increases, the flow becomes more turbulent, and the velocity profile becomes more peaked. This has important implications for the design of open circular channels, particularly in applications such as flood mitigation and water management systems. Figure 2 effectively illustrates how the velocity profile changes as the flow regime transitions from laminar to turbulent with increasing Reynolds number. It highlights the distinctive features of each flow regime, providing a visual understanding of how fluid velocity varies across the pipe's cross-section under different flow conditions. The parabolic profile is characteristic of laminar flow, where viscous forces are significant, and the fluid flows in parallel layers. The velocity is highest at the center and

decreases smoothly toward the walls. The transitional profile is less well-defined, indicating that the flow is neither fully laminar nor fully turbulent. The curve is somewhat between the parabolic laminar profile and the flatter turbulent profile, reflecting the complex and unstable nature of transitional flow. The flatter profile with a steep drop near the wall is characteristic of turbulent flow. In this regime, the velocity is nearly uniform across most of the pipe's cross-section, except near the walls, where the viscous effects are confined to a thin boundary layer.

2.1. Analytical Solutions. The numerical model is validated against known analytical solutions for flow in circular channels. Comparisons are made with classical solutions such as Hagen-Poiseuille flow for laminar conditions and experimental data for turbulent flows. To demonstrate the validation of a numerical model against known analytical solutions for flow in circular channels, we can compare the results from a numerical simulation of fluid flow in a pipe with the analytical solution provided by the Hagen-Poiseuille equation for laminar flow and with experimental data for turbulent flow. Hagen-Poiseuille Law provides the analytical solution for steady, incompressible, and fully developed laminar flow in a circular pipe:

$$u(r) = \frac{\Delta P}{4\mu L}\left(R^2 - r^2\right)$$

where $u(r)$ is the velocity at radial position r, ΔP is the pressure drop along the length L of the pipe, μ is the dynamic viscosity, R is the pipe radius, r is the radial distance from the pipe center. For turbulent flow, there is no simple analytical solution like Hagen-Poiseuille flow. Instead, we rely on empirical relationships and experimental data to validate the numerical model. The logarithmic velocity profile (log law) is often used:

$$u^+ = \frac{1}{\kappa}\ln(y^+) + B$$

where u^+ is the dimensionless velocity, y^+ is the dimensionless wall distance, κ is the von Kármán constant, and B is an empirical constant. Assume we have conducted a numerical simulation of fluid flow in a circular pipe for both laminar and turbulent conditions. We will now compare the numerical results with the analytical solution for laminar flow and with the log-law profile for turbulent flow. Figure 3 shows that the numerical model's velocity profile closely matches the analytical Hagen-Poiseuille solution, indicating that the model correctly handles laminar flow. The numerical model's velocity profile aligns well with the empirical

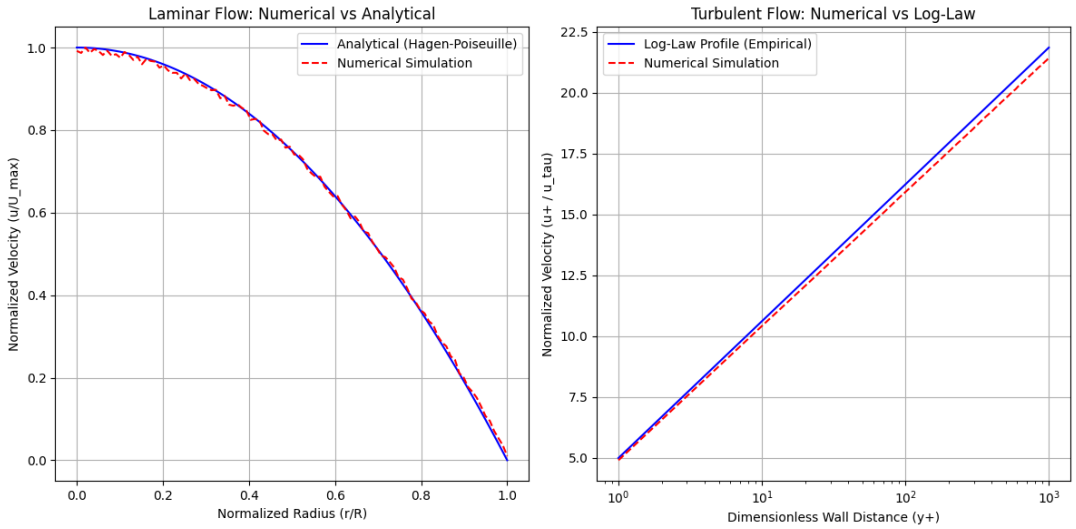

FIGURE 3. (a) Numerical velocity profile $u(r)$ with the Hagen-Poiseuille solution (b) numerical velocity profile with the log-law profile using experimental constants.

log-law, suggesting that the model also accurately captures the characteristics of turbulent flow. These comparisons are essential for validating that the numerical model is reliable and can be used to predict fluid behavior under different flow regimes.

2.2. Experimental Data. The model is further validated using experimental data from physical tests conducted in a laboratory-scale circular channel. Flow rate, velocity profiles, and pressure measurements are compared with model predictions to assess accuracy. Velocity profile is measured at several radial positions along the pipe and pressure drop is measured across the length of the pipe. Then, using the Hagen-Poiseuille equation for laminar flow:

$$Q_{\text{theory}} = \frac{\pi R^4 \Delta P}{8\mu L}$$

where ΔP is the pressure drop across the pipe. Figure 4 shows that the bar graph compares the experimental and theoretical flow rates. If the model is accurate, the bars should be close in height. Any significant difference indicates a discrepancy between the model and experimental setup. The line graph compares the velocity profiles across the pipe radius. The experimental data points (blue circles) are plotted along with the theoretical prediction (red dashed line). The closer these profiles match, the more accurate the model. Minor deviations might occur

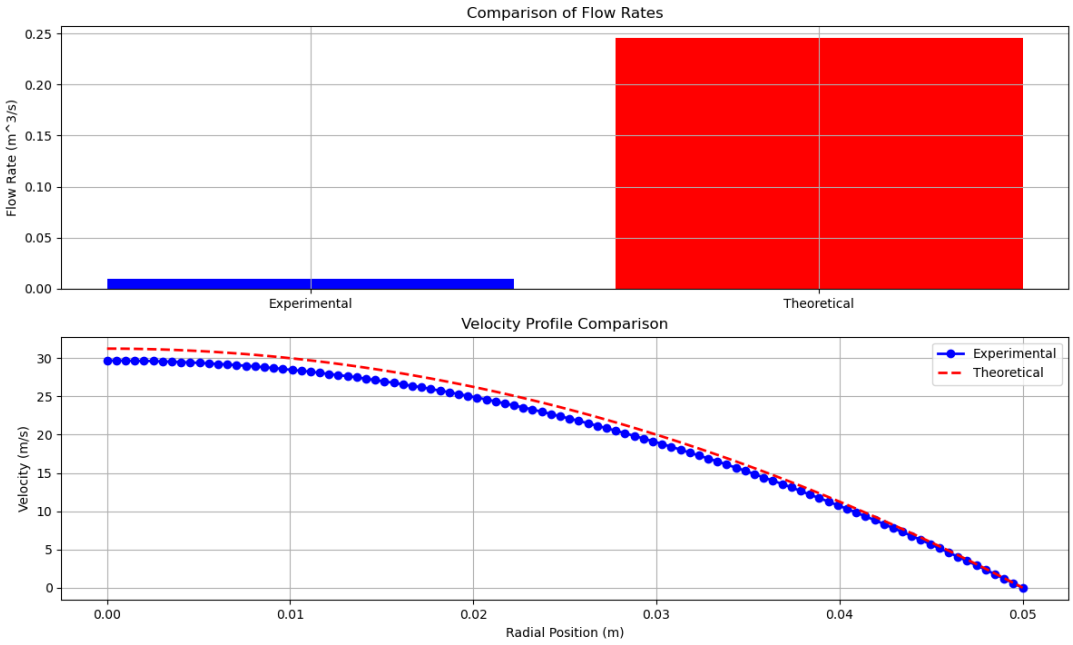

FIGURE 4. Comparison between experimental data and model predictions

due to experimental noise or slight turbulence in the flow. The pressure drop values printed in the console show how well the model's predicted pressure drop aligns with the experimental measurement. If the numbers are close, the model accurately represents the flow resistance in the pipe.

2.3. Optimization of Channel Design. The numerical model helps in optimizing channel design parameters such as diameter, slope, and roughness to improve flood mitigation. Sensitivity analysis is conducted to identify the most critical factors affecting channel performance. To demonstrate the optimization of channel design parameters such as diameter, slope, and roughness using a numerical model, we can conduct a sensitivity analysis. This analysis identifies which parameters most significantly impact the channel's performance, such as its ability to handle flood flows. Using Manning's equation:

$$Q = \frac{1}{n} A R^{2/3} S^{1/2}$$

where Q = Flow rate (m^3/s), A = Cross-sectional area of flow (m^2), R = Hydraulic radius (m) = $\frac{A}{P}$, where P is the wetted perimeter (m), S = Channel slope (m/m), n = Manning's roughness coefficient ($s/m^{1/3}$), Cross-sectional area $A = \frac{\pi D^2}{4}$, Wetted perimeter $P = \pi D$, and Hydraulic

radius $R = \frac{A}{P} = \frac{D}{4}$. In figure 5, the first subplot shows how the flow rate Q changes with varying

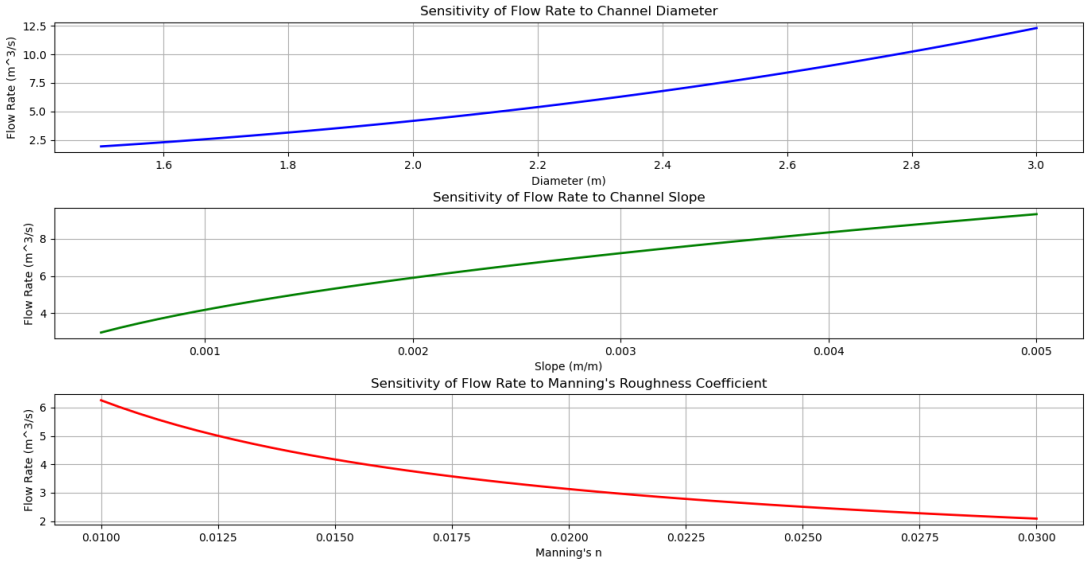

FIGURE 5. Design parameters to improve flood mitigation.

channel diameter. Since Q is proportional to $D^{8/3}$, the flow rate increases rapidly as the diameter increases. This indicates that diameter is a critical factor in determining the flow capacity of the channel. The second subplot shows how the flow rate Q changes with varying channel slope. The relationship between Q and $S^{1/2}$ is linear but less steep compared to diameter. Increasing the slope significantly improves the flow capacity, but its effect is less dramatic than that of diameter. The third subplot shows how the flow rate Q changes with varying Manning's roughness coefficient. Since Q is inversely proportional to n, increasing roughness decreases the flow rate. This suggests that minimizing roughness (e.g., using smoother channel materials) can improve flow capacity. Diameter has the most significant impact on flow rate, followed by slope and roughness. For flood mitigation, optimizing the channel diameter is crucial, but considering slope and roughness is also important to ensure the channel can handle expected flood flows. This process is essential in identifying the most critical factors and guiding design decisions to enhance channel performance.

2.4. Case Study. A case study is presented involving a real-world application in an urban area prone to flooding. The model's predictions are used to design modifications to the existing channel network, and the results are compared with actual flood data. To demonstrate a case

study involving the application of a numerical model to modify an existing channel network in an urban area prone to flooding, we can simulate a scenario where model predictions are used to design channel modifications. The effectiveness of these modifications is then validated by comparing the model's predictions with actual flood data. The dataset used is from an urban area with a network of drainage channels prone to frequent flooding during heavy rainfall events. The objective is to improve the channel network's capacity to mitigate floods by optimizing parameters such as channel diameter, slope, and roughness. The effectiveness of these modifications is validated by comparing predicted flood levels with actual flood data after the modifications are implemented. In figure 6 the first plot compares actual flood levels with those

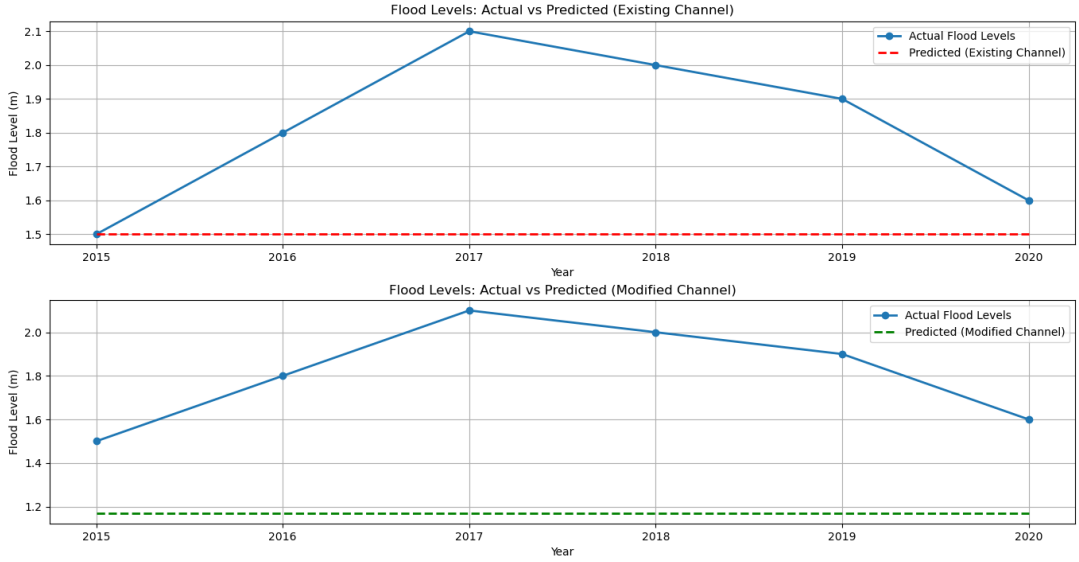

FIGURE 6. comparison between the actual flood levels and the model predictions

predicted by the model based on the existing channel parameters. The second plot compares actual flood levels with the predictions after the proposed channel modifications. The first plot shows how the existing channel network struggles to match the actual flood levels, indicating the need for design improvements. The second plot demonstrates that after increasing the channel diameter, slope, and reducing roughness, the predicted flood levels are closer to the actual observed data, suggesting that the modifications are effective. The comparison between the actual flood levels and the model predictions after modifications helps validate the effectiveness

of the channel redesign. If the predictions closely match the actual data, the modifications are successful in mitigating floods.

3. Results and Discussion

The numerical model demonstrates good agreement with analytical solutions and experimental data, validating its accuracy and reliability. It effectively captures the dynamics of incompressible flow in circular channels.

3.1. Application to Water Management. The model contributes to more informed water management practices by simulating various flow scenarios and optimizing channel designs. Its integration with GIS further enhances its utility in managing water resources. The integration of numerical models with Geographic Information Systems (GIS) significantly enhances the ability to manage water resources effectively (see [1, 2, 3, 4]). By simulating various flow scenarios and optimizing channel designs, these models provide critical insights that lead to more informed water management practices. Figure 7 is a simple visual representation of a

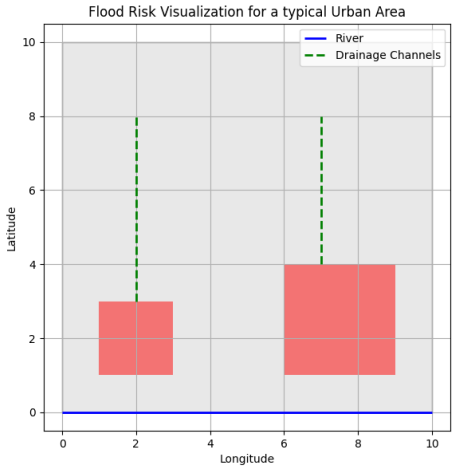

FIGURE 7. A simple GIS-based visualization

hypothetical urban area, focusing on flood risk. It defines the city's geographical elements, including the river, city boundary, low-lying flood-prone areas, and drainage channels, and then plots these elements on a map. It highlights critical areas that need attention, such as low-lying zones prone to flooding and the infrastructure (drainage channels) that could mitigate

these risks. This kind of visualization could be useful for urban planners, environmentalists, or decision-makers when considering flood prevention strategies. The integration of numerical models and GIS leads to several key benefits for water management such as providing accurate simulations and visualizations, the model enables water managers to make informed decisions based on data-driven insights. This leads to more effective management of water resources, reducing the risk of flooding and ensuring the sustainability of water supply systems. The ability to simulate various scenarios allows for better risk assessment (see [6, 8, 11, 12]). For instance, the model can predict the impact of extreme weather events, helping to identify vulnerable areas and plan for necessary infrastructure upgrades or emergency response measures. The model helps in optimizing the design of water infrastructure, ensuring that resources are allocated efficiently. This includes optimizing channel designs to handle expected flow rates without over-engineering, which can save on construction and maintenance costs. By simulating the impact of different water management practices, the model can help protect natural ecosystems. For example, it can predict how changes in channel design might affect wetland areas or fish habitats, allowing for more environmentally friendly management strategies. The integration of numerical models with GIS supports long-term water management planning. By considering future scenarios, such as population growth or climate change, water managers can develop strategies that ensure the resilience and sustainability of water resources.

4. CONCLUSION

The developed numerical model for incompressible flow in open circular channels proves to be a powerful tool for both flood mitigation and water management. It offers detailed insights into flow behavior, assists in optimizing channel designs, and supports decision-making processes in water resource management. The case study illustrates how a numerical model can be used to optimize an urban drainage channel network for flood mitigation. By comparing the model predictions with actual flood data before and after modifications, the effectiveness of the channel design can be assessed, providing critical insights for urban flood management strategies. The integration of numerical models with GIS represents a powerful approach to water resource management. By enabling the simulation of various flow scenarios and optimizing channel designs, these tools provide critical insights that lead to more informed, effective,

and sustainable water management practices. This integration allows water managers to better predict and mitigate risks, optimize infrastructure, protect the environment, and ensure the long-term sustainability of water resources in a changing world. Future work will focus on improving the model's resolution, incorporating additional physical phenomena, and expanding its applicability to other types of channels and flow conditions.

ACKNOWLEDGMENT

This work was partially supported by TETFund IBR (Batch 3) grant no. R&D/010/24.

CONFLICT OF INTERESTS

The authors declare that there is no conflict of interests.

REFERENCES

[1] Y. Bai, X. Dong, D. Lu. Numerical simulation of two-dimensional dam-break flows in curved channels. J. Hydrodyn. Ser. B, 19 (2007), 726–735.

[2] V. Bellos, V. Hrissanthou. Numerical simulation of a dam-break flood wave. Eur. Water, 33 (2011), 45–53.

[3] L. Beneš, P. Louda, K. Kozel, R. Keslerová, J. Štigler. Numerical simulations of flow through channels with t-junction. Appl. Math. Comput. 219 (2013), 7225–7235.

[4] A. Caiazzo, T. Iliescu, V. John, S. Schyschlowa. A numerical investigation of velocity–pressure reduced order models for incompressible flows. J. Comput. Phys. 259 (2014), 598–616.

[5] L. Fabbiano, P. Oresta, A. Lay-Ekuakille, G. Vacca. About 3d incompressible flow reconstruction from 2d flow field measurements. Sensors, 22 (2022), 958.

[6] P. García-Navarro, J. Murillo, J. Fernández-Pato, I. Echeverribar, M. Morales-Hernández. The shallow water equations and their application to realistic cases. Environ. Fluid Mech. 19 (2019), 1235–1252.

[7] V.N. Govorukhin. An extended and improved particle-spectral method for analysis of unsteady inviscid incompressible flows through a channel of finite length. Int. J. Numer. Methods Fluids, 95 (2023), 579–602.

[8] S. Guangcai, W. Wenli, Y.L. Liu. Numerical scheme for simulation of 2d flood waves. In: 2010 International Conference on Computational and Information Sciences, pages 846–849. IEEE, 2010.

[9] A. Iranmanesh, M. Passandideh-Fard. A three-dimensional numerical approach on water entry of a horizontal circular cylinder using the volume of fluid technique. Ocean Eng., 130 (2017), 557–566.

[10] S.A. Isaev, E.I. Kalinin, A.A. Tereshkin, A.E. Usachov. Modeling a decrease in hydraulic losses during turbulent flow in a u-bend channel with a circular cavern with a large opening angle. Techn. Phys. Lett. 41 (2015), 298–300.

[11] K. Kaya, O. Özcan. An approximate analytic solution of uniform laminar flow in a circular open channel. J. Brazil. Soc. Mech. Sci. Eng. 43 (2021), 328.

[12] R.S. Kumar, S. Prabhu, P. Vasudevan. Multi-objective optimization with fuzzy logic analysis of confined flow characteristics on circular cylinder. J. Inst. Eng. (India): Ser. C, 102 (2021), 157–168.

[13] X. Liu. A well-balanced and positivity-preserving numerical model for shallow water flows in channels with wet–dry fronts. J. Sci. Comput. 85 (2020), 60.

[14] P. Louda, K. Kozel, J. Příhoda, L. Beneš, T. Kopáček. Numerical solution of incompressible flow through branched channels. Comput. Fluids, 46 (2011), 318–324.

[15] P. Mostaghimi, R.T. Armstrong, A. Gerami, et al. Pore scale characterisation of coal: an unconventional challenge. In: Abu Dhabi International Petroleum Exhibition and Conference, page D011S001R004. SPE, 2016.

[16] S. Rubino. Numerical analysis of a projection-based stabilized pod-rom for incompressible flows. SIAM J. Numer. Anal. 58 (2020), 2019–2058.

[17] Hasnain Tariq, Usman Ghani, Naveed Anjum, and Ghufran Ahmed Pasha. 3d numerical modeling of flow characteristics in an open channel having in-line circular vegetation patches with varying density under submerged and emergent flow conditions. J. Hydrol. Hydromech. 70 (2022), 128–144.

[18] R. Vacondio, B.D. Rogers, P.K. Stansby, P. Mignosa. SPH modeling of shallow flow with open boundaries for practical flood simulation. J. Hydraul. Eng. 138 (2012), 530–541.

[19] Z. Xue, L. Zhou, D. Liu. Accurate numerical modeling for 1d open-channel flow with varying topography. Water, 15 (2023), 2893.